Optik - International Journal for Light and Electron Optics 195 (2019) 163027

Contents lists available at ScienceDirect

Optik

journal homepage: www.elsevier.com/locate/ijleo

Original research article

On the impact of LED power uncertainty on the accuracy of 2D and 3D Visible Light Positioning

David Plets[a,*], Sander Bastiaens[a], Luc Martens[a], Wout Joseph[a], Nobby Stevens[b]

[a] Ghent University/imec, Dept. of Information Technology, Technologiepark 126, B-9052 Ghent, Belgium
[b] KULeuven-DraMCo, Gebroeders De Smetstraat 1, B-9000 Ghent, Belgium

ARTICLE INFO

Keywords:
VLP
RSS
2D
3D
Fingerprinting
Trilateration
Transmit power
LED

ABSTRACT

This paper presents a simulation study of the impact of Light Emitting Diode (LED) output power uncertainty on the accuracy of Received Signal Strength (RSS)-based two-dimensional (2D) and three-dimensional (3D) Visible Light Positioning (VLP). The actual emitted power of a LED is never exactly equal to the value that is tabulated in the datasheet, with possible variations (or tolerances) up to 20%. Since RSS-based VLP builds on converting estimated channel attenuations to distances and locations, this uncertainty will impact VLP accuracy in real-life setups. For 2D, a typical configuration with four LEDs is assumed here, and a Monte-Carlo simulation is executed to investigate the distribution of the resulting positioning errors for four tolerance values at seven locations. It is shown that median errors are the highest just below the LEDs, when using a traditional Least-Squares minimization metric. When tolerance values on the LED power increase from 5% to 20%, median errors vary from at most 2 cm to at most 10 cm. Maximal errors can be as high as 17 cm just below the LED, already for tolerance values of only 5%, and increase up to 40 cm for tolerance values of 20%. An alternative cost metric using normalized Least-Squares minimization makes the errors spatially more homogeneously distributed and reduces them by 35%. For a 3D case, median errors of around 5 cm for a tolerance value of 5% increase to as much as 22 cm for a tolerance value of 20%. As the receiver heights increase, positioning errors decrease significantly.

1. Introduction

The introduction of Light Emitting Diodes (LEDs) has not only revolutionized the lighting world thanks to the increased energy efficiency and lifetime compared to traditional lighting bulbs, but it has also unlocked new applications. The ability to modulate the emitted light signal allows transmitting data, a technology known as Visible Light Communication (VLC) [1]. Another promising application of visible light is Visible Light Positioning (VLP) [1,2], where e.g., the location of a photodiode (PD) is estimated. Advantages over well-known Radio-Frequency (RF) solutions, such as Ultra-Wide-Band (UWB) Time-of-Arrival (ToA)-based positioning [3], Angle-of-Arrival (AoA)-based positioning, or Received Signal Strength Indicator (RSSI)-based location tracking [4], include achieving high positioning accuracies while maintaining a low deployment cost. Similarly to RF solutions, VLP can use AoA or RSS-based approaches. The latter approach is often preferred thanks to the lower complexity of the receiver. It builds on the link between observed light intensities and distances between the LED source and the receiving photodiode, using (or assuming) knowledge of the visible light channel attenuation as a function of distance. However, such conversion also requires exact knowledge

* Corresponding author.
E-mail address: david.plets@ugent.be (D. Plets).

https://doi.org/10.1016/j.ijleo.2019.163027
Received 26 February 2019; Received in revised form 6 June 2019; Accepted 27 June 2019

of the LED characteristics. E.g., in [5], the impact of the LED beam profile is investigated, while in [6], the transmitter semi-angle and spatial LED configuration are optimized. Also in [7], the impact of the Lambertian order on positioning accuracy is investigated. Next to more common research on the impact and correction of receiver tilt in VLP [8], work in [9] studied the impact of LED tilt on VLP accuracy. Another important factor in the visible light link is transmitted power of each of the LEDs. Research in [10] investigated the optimal allocation of LED powers in a VLP system. In reality, the precision of these powers is limited, and uncertainties typically amount to around 5% [11]. For Chips on Board (COBs) LEDs, tolerances are up to ± 10% [12], and for some LED manufacturers, uncertainties could be as high as 20%. To the authors' knowledge, up to now, no research efforts have been made to characterize the impact of this uncertainty on the performance of VLP in terms of accuracy. In [13], the authors presented the impact of LED power uncertainty for a simple two-dimensional (2D) configuration. This paper will extend this research and proposes an alternative metric to reduce this impact. Further, it will also assess the impact for a three-dimensional (3D) VLP configuration [14]. A Monte-Carlo simulation will be executed, in which it is assumed that each of the four deployed LEDs has a certain unknown (and uncorrelated) deviation on its assumed output power. This way, the positioning error will be characterized for different locations within the test site, and for four different tolerance values (5, 10, 15, and 20%).

Section 2 will present the visible light channel model that will be used in the positioning algorithm. In Section 3, the simple VLP test setups that will be assumed for the simulations, will be discussed, while Section 4 will present the 2D and 3D positioning algorithms. Results will be discussed in Section 5, and the main findings of this work will be summarized in Section 6.

2. Channel model

In this work, only the Line-of-Sight (LoS) path between the transmitting LED source and the receiving PD will be assumed. Reflections are not considered as a source of 'measurement noise', in order to be able to unambiguously assess the effect of only the tolerance on the LEDs' output powers, and to compare both effects. For the same reason, no actual noise (e.g., shot noise or thermal noise) is initially considered in this study. The model parameters of the visible light channel are displayed in Fig. 1. The power P_R received at the photodiode is calculated according to the channel model used in [15]:

$$P_R = P_E \cdot h_{\text{LoS}}, \tag{1}$$

with P_E the emitted optical power by the LED, which will thus be statistically distributed in this paper. h_{LoS} is the channel gain along the direct link and can be described as follows [15]:

$$h_{\text{LoS}} = R_E(\phi, \gamma) \cdot \frac{A_{\text{eff}}(\psi)}{d^2} \cdot T_R(\psi) \cdot G_R(\psi), \tag{2}$$

where $R_E(\phi, \gamma)$ is the radiation pattern of the LED, with ϕ the angle of irradiance (see Fig. 1) and γ the azimuthal angle. In case of a Lambertian emitter, the radiation pattern is axially symmetric and for order m, reduces to $\frac{m+1}{2\pi}\cos^m(\phi)$. $T_R(\psi)$ and $G_R(\psi)$ are the optical filter's gain and the optical concentrator's gain at the receiver respectively, with ψ the angle of incidence. The field-of-view (FOV) of the photodiode is two times ψ_C (see Fig. 1), such that h_{LoS} becomes equal to zero for $|\psi| > \psi_C$. Within the FOV of the PD, $T_R(\psi)$ and $G_R(\psi)$ will be assumed equal to 1 in the following. It will further be assumed that the PD's FOV is sufficiently large to record the signals from all LEDs within the configuration. In addition, both the LED and PD orientation will be assumed horizontal,

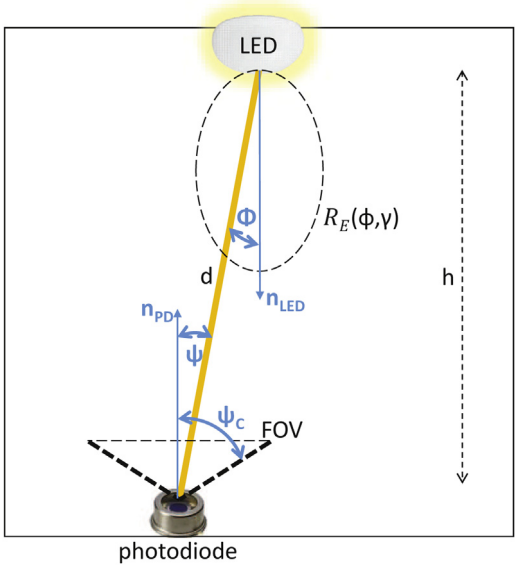

Fig. 1. Overview of visible light channel and the involved parameters.

corresponding to their respective normal vectors $\vec{n}_{\mathrm{LED}}$ and $\vec{n}_{\mathrm{PD}}$ being parallel. In this case, the angle of irradiance $\phi = \psi$ (see Fig. 1), with $\cos(\phi) = \cos(\psi)$ being equal to h/d, with h the height difference between the LED and the PD, and d the distance between the LED and the PD. A_{eff} is the effective photodiode area, which is equal to the photodiode area that is perpendicular to the angle of incidence ψ:

$$A_{\mathrm{eff}}(\psi) = A_R \cdot \cos(\psi), \tag{3}$$

with A_R the actual photodiode area, here equal to 1 cm^2. For a Lambertian emitter, Eq. (1) can be rewritten as [15]:

$$P_R = P_E \cdot \frac{m+1}{2\pi d^2} \cdot \cos^m(\phi) \cdot A_R \cdot \cos(\psi). \tag{4}$$

3. Simulation configuration

3.1. 2D configuration

The simulation tests for the 2D case will be executed for the room that is depicted in Fig. 2a. The dimensions of the room are 5 m × 5 m, with a ceiling height of 2.5 m. The Lambertian order m of the LEDs, each of which is horizontally oriented, is equal to 1, for all four LEDs. The receiver PD is also assumed to be horizontally oriented, at a height of 0.85 m. In this 2D scenario, we assume that the receiver height is fixed and known (representing a use case where e.g., a cart with a PD on top is being moved around), reducing the estimation of the receiver location to a planar problem. A receiver grid of 2 mm will be considered here, meaning that the PD center can be located at $N_L = 2500^2$ locations. Further, we assume that the receiver hardware is able to demultiplex the contributions of the different LED sources [16]. Four LEDs with an assumed optical power of 10 W are attached to the ceiling (h = 2.5 m), at the locations indicated in Fig. 2. However, in reality, the emitted power P_{Ei} of LED_i ($i = 1 \ldots N$) will be normally distributed around the value of 10 W:

$$P_{\mathrm{Ei}} \sim \mathcal{N}(10,\ \sigma^2).$$

In this study, four tolerance values T_{LED} will be tested: ± 5%, ± 10%, ± 15%, and ± 20%. These tolerance values typically refer to 3-sigma deviations, meaning that the standard deviations σ of these normal distributions around the 10 W-value will correspond to 0.167 W, 0.333 W, 0.5 W, and 0.666 W, respectively. Further, it will be assumed that there is no correlation between the deviations of the transmit power value of the different LEDs in the room.

Fig. 3a shows the seven positions at which the location will be estimated. Thanks to the 8-fold symmetry of the setup, only locations within the triangle A–C–E need to be considered, since the statistical distribution of the positioning errors will repeat itself at the corresponding locations of the different parts of the 5 m × 5 m area. It should be noted though that each single simulation will result in an asymmetric setup, since for each simulation, the power of each LED will be randomly and independently chosen. However, the resulting distribution at corresponding locations will be the same when enough simulations are considered, due to the fact that the statistical distribution of the LED power is the same for each of the LEDs. Table 1 shows the coordinates of each of the positions A–G, where A is set at the center of the coordinate system, and G is the centroid of the triangle formed by the other points (see Fig. 3a).

In this work, a position estimation for each of the seven positions (A–G) will be executed for 10 000 random sets of LED power values (P_{E1}, P_{E2}, P_{E3}, …, P_{EN}) in the Monte-Carlo simulation (N = 4 here). Each position estimation will be done according to the algorithm presented in Section 4.1.

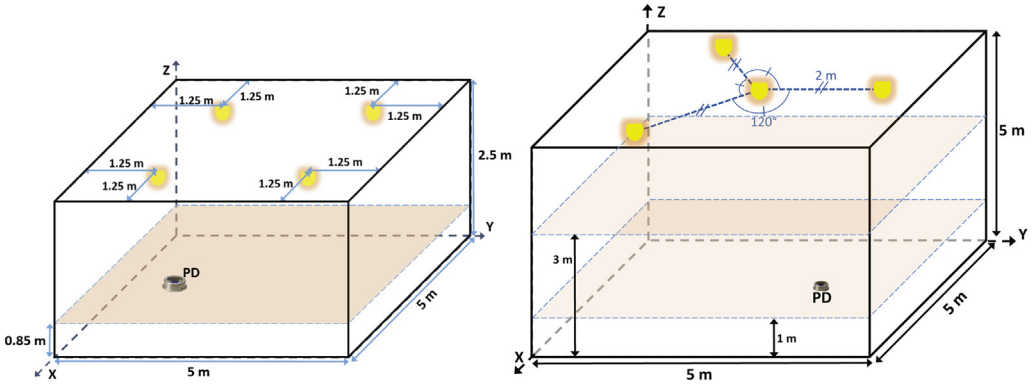

(a) 2D setup (b) 3D setup

Fig. 2. Overview of the simulation setup.

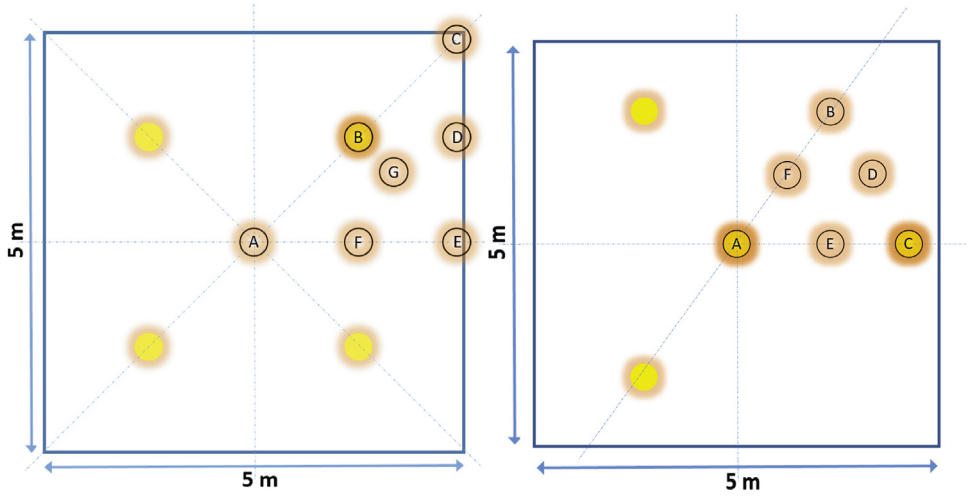

(a) 2D setup (b) 3D setup

Fig. 3. Top view of the simulation setups, with indication of the four LEDs (yellow dots) and the seven (2D) or six (3D) locations (letters, see Table 1) for which the positioning error will be evaluated. (For interpretation of the references to color in this figure legend, the reader is referred to the web version of this article.)

Table 1
Coordinates (m) of the considered locations, where A is set at the center of the coordinate system, the *x*-axis pointing rightwards, and the *y*-axis pointing upwards (see Fig. 3).

2D configuration (see Fig. 3a)							
Location	A	B	C	D	E	F	G
(*x*,*y*)	(0,0)	(1.25,1.25)	(2.25,2.25)	(2.25,1.25)	(2.25,0)	(1.25,0)	(1.67,0.83)

3D configuration (see Fig. 3b)						
Location	A	B	C	D	E	F
(*x*,*y*)	(0,0)	$(1, \sqrt{3})$	(2,0)	$\left(1.5, \frac{\sqrt{3}}{2}\right)$	(1,0)	$\left(0.5, \frac{\sqrt{3}}{2}\right)$

3.2. 3D configuration

Similarly to the 2D configuration, the 3D configuration is a 5 m × 5 m room, where the LEDs' Lambertian mode m equals 1, and their optical powers are again normally distributed around their assumed nominal value of 10 W. However, the assumed LED height h_{LED} is 5 m here, i.e., the ceiling height. Fig. 2b depicts the considered area, where the PD height is not known a priori here. Further, the LEDs are not mounted in the typical square configuration of Fig. 2a, as such configuration does not allow an unambiguous 3D position estimate, as shown in [17]. Instead, we opt for the star-shaped configuration of Fig. 2b, where 3 LEDs are located around one central LED, each at a distance of 2 m. The PD and all LEDs are horizontally oriented. Fig. 3b shows the six positions at which the location will be estimated via a Monte-Carlo simulation. Again, thanks to the 6-fold symmetry of the setup, only locations within the triangle A–B–C are considered here. Table 1 shows the coordinates of each of the positions A–F, where A is set at the center of the coordinate system, and D, E, and F are the middles of the triangle sides. Besides the LEDs located at A and C, the two other LEDs have coordinates $(-1, \sqrt{3})$ and $(-1, -\sqrt{3})$. Similarly to the 2D case, a position estimation for each of the six positions (A to F) will be executed for 10 000 random sets of LED power values in the Monte-Carlo simulation. Each position estimation will be done according to the algorithm presented in Section 4.2. The procedure will be executed at a height of 0.85 m (same as 2D case) and at a height of 3 m, in order to compare the influence of the receiver height.

4. Positioning algorithm

4.1. 2D positioning algorithm

The adopted positioning algorithm is based on a commonly used Least-Squares minimization [4]. It compares the set of observed received photodiode powers $P_{\mathrm{Ri}}^{\mathrm{obs}}$ from each LED_i ($i = 1, \ldots, N$) at the unknown PD location, with the set of fingerprinted PD powers

$P_{\mathrm{Ri}}^{L,\mathrm{model}}$ from LED_i at all (2500^2) locations L in the grid. Observations can either be simulations or actual measurements. For the construction of the fingerprinting database of the $P_{\mathrm{Ri}}^{L,\mathrm{model}}$ values, P_E is assumed equal to 10 W for each LED, as it is the most probable value for P_E. The set of observations (P_{R1}^{obs}, P_{R2}^{obs}, P_{R3}^{obs}, ..., $P_{\mathrm{RN}}^{\mathrm{obs}}$) represent the observed values in the realistic setup investigated here. They are obtained from (P_{E1}, P_{E2}, P_{E3}, …, P_{EN}), where P_{Ei} values are obtained as samples from $\mathcal{N}(10,\ \sigma^2)$. The larger the uncertainty on the P_{Ei} values (larger σ^2 values), the larger the positioning errors will be.

The algorithm estimates the unknown location L to be at the spot where the cost function C_{square}^{L} has a minimum [18]:

$$C_{\mathrm{square}}^{L} = \sum_{i}^{N} (P_{\mathrm{Ri}}^{\mathrm{obs}} - P_{\mathrm{Ri}}^{L,\mathrm{model}})^2. \tag{5}$$

Each position estimation thus consists of a comparison of the set of observations (P_{R1}^{obs}, P_{R2}^{obs}, ...,$P_{\mathrm{RN}}^{\mathrm{obs}}$) against all ($P_{R1}^{L,\mathrm{model}}$, $P_{R2}^{L,\mathrm{model}}$, ...,$P_{\mathrm{RN}}^{L,\mathrm{model}}$) sets that are stored in the database. In total, N_L sets of N values of $P_{\mathrm{Ri}}^{L,\mathrm{model}}$ are precalculated and stored in a fingerprinting database, i.e., the received power at N_L locations from each of the N LEDs, according to the LoS channel model from Section 2. For the configuration under test, $N = 4$ and $N_L = 2500^2 = 6\,250\,000$, meaning that 25 million values are stored. It is clear that more advanced search algorithms will be useful here, in order to quickly find the location with the lowest C_{square}^{L}.

4.2. 3D positioning algorithm

While the 2D positioning algorithm is based on a model-based fingerprinting approach with a 2 mm granularity [4,19], this approach becomes unfeasible in 3D due to the requirement of large memory and computation time to iterate over the 3D map. In 3D, we use the trilateration method from [17] where the 3D position could be quickly retrieved, solely based on the observed PD powers and without any prior knowledge of the PD receiver height. It is based on an iterative 2D trilateration where different candidate PD receiver heights are evaluated based on a cost function which, at its minimum value, yields the received position. The positioning algorithm is summarized in the following.

Given an observed power $P_{\mathrm{Ri}}^{\mathrm{obs}}$ from LED_i ($i = 1, \ldots, 4$) and knowing that $\cos(\phi_i) = \cos(\psi_i) = \frac{h}{d_i}$ for horizontally oriented LEDs and PD (see Fig. 1), Eq. (4) can be rewritten to allow the calculation of the estimated distance $\hat{d}_i$ between LED_i and PD:

$$\hat{d}_i = \sqrt[m+3]{(m+1)\cdot\frac{P_E}{2\pi P_{\mathrm{Ri}}}\cdot h^{m+1}\cdot A_R}\,. \tag{6}$$

For each possible height difference h between the LEDs and the PD, a 2D trilateration is then performed, leading to a set of candidate 3D position estimates ($\hat{x}(h)$, $\hat{y}(h)$, $h_{LED} - h$), one per evaluated height difference h. Finally, each of these candidate positions is evaluated based on a cost function $C(h)$, comparing estimated LED–PD distances at the assumed height difference h with LED–PD distances at the 3D estimated position at that height difference. The height difference $h = h^*$ that produces a minimum value $C(h)$, yields the 3D position estimate ($\hat{x}(h^*)$, $\hat{y}(h^*)$, $h_{LED} - h^*$) [17].

$$C(h) = \frac{1}{4}\sum_{i=1}^{4} [\hat{d}_i(h) - \sqrt{(\hat{x}(h) - x_i)^2 + (\hat{y}(h) - y_i)^2 + h^2}]^2, \tag{7}$$

with (x_i, y_i, h_{LED}) the coordinates of LED_i, $i = 1 \ldots 4$ for the configuration depicted in Fig. 2b. Candidate receiver PD heights between 25 cm and 3.5 m will be considered here, with a granularity of 2 mm.

5. Results

5.1. 2D positioning

Table 2 lists the median (p_{50}) and 95%-percentile (p_{95}) values of the positioning errors that are obtained from 10^4 simulations in each of the locations A to G in Fig. 3a, for tolerances T_{LED} of ± 5%, ± 10%, ± 15%, and ± 20%, respectively. For T_{LED} = 5%, median errors are 2.3 cm at most (C). Maximal errors are limited to 5.6 cm (C), except in location B, where the maximal error amounts to

Table 2
Median (p_{50}) and maximal (p_{95}) errors (cm) at each of the seven locations A–G (see Fig. 3a) for four tolerance values T_{LED} of the LEDs.

T_{LED}		A	B	C	D	E	F	G
5%	p_{50}	1.2	1.7	2.3	1.9	1.6	1.4	2.2
	p_{95}	2.4	17.6	5.6	4.1	3.5	4.4	5.2
10%	p_{50}	2.3	3.3	4.7	3.8	3.3	2.7	4.4
	p_{95}	4.7	26.7	10.9	8.2	6.9	20.3	10.4
15%	p_{50}	3.4	4.5	7.1	5.7	5.0	4.7	6.7
	p_{95}	7.1	33.8	15.8	12.7	10.5	30.0	15.6
20%	p_{50}	4.6	5.6	9.5	7.6	6.5	6.6	9.0
	p_{95}	9.6	40.1	18.7	16.6	13.8	37.5	20.6

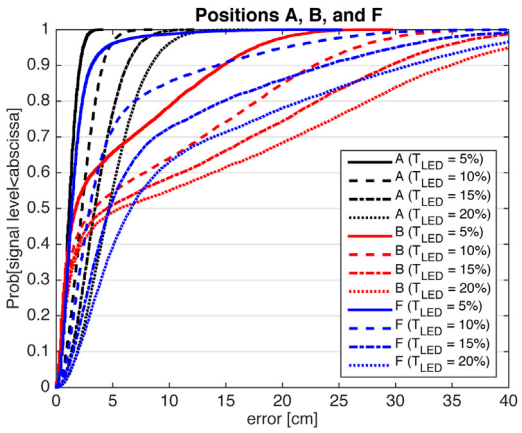

Fig. 4. Cdfs of the errors obtained from 10 000 simulations at the locations A, B, and F for all four LED tolerance values.

17.6 cm.

All median errors scale more or less linearly with the tolerance values: the errors increase by approximately 100, 200, and 300%, when T_{LED} increases from 5% to 10, 15, and 20%, respectively. For these positions, median errors (p_{50}) vary between 2 and 5 cm for T_{LED} = 10%, 3–7.5 cm for T_{LED} = 15%, and between 4 and 10 cm for T_{LED} = 20%. Apart from positions B and F, maximal errors (p_{95}) also show a more or less linear increase: values from 2.5 to 5 cm for T_{LED} = 5%, from 5 to 10 cm for T_{LED} = 10%, 7 to 15 cm for T_{LED} = 15%, and between 10 and 20 cm for T_{LED} = 20% are observed. Moreover, p_{95} values are between 2 and 2.5 times as high as the median errors for all values of T_{LED}.

As mentioned earlier, maximal errors at location B are at least three times as high as at other locations for T_{LED} = 5%. Although this error does not increase at the same rate as for the other locations when T_{LED} increases, p_{95} is still at least twice as high as at the other locations for T_{LED} = 20%. Maximal errors at location F are in line with the other locations for T_{LED} = 5%, but for higher T_{LED} values ($\geq$10%), a trend similar to that at location B is observed: a large portion of the LED configurations leads to remarkably higher errors compared to locations A–C–D–E–G. In general, position A (middle of the room, middle between the four LEDs) shows the lowest median ($<$ 5 cm) and maximal ($<$ 10 cm) errors.

Fig. 4 collects for positions A, B, and F the cumulative distribution functions (cdfs) of the errors for the four values of T_{LED}, where the x-axis has been limited to 40 cm for reasons of clarity. It shows that for position A (black curves), the errors increase in a regular way as T_{LED} increases. The same counts for position F (blue curves), but the increase of the errors is significantly larger. Finally, for position B (red curves), it can be seen that the smallest 40% of the errors is affected in a very limited way as T_{LED} increases, and that these errors are lower than at positions A and F. However, the largest half of the errors in B is (significantly) larger than in A (and F).

In order to gain more insight into this position-dependency of the error, the errors for T_{LED} = 10% within the top right quarter of Fig. 3 (square formed by sides AE and CE) have been simulated on a denser grid of 50 by 50 positions, but due to calculation time, for only 100 instead of 10 000 simulations per position. Since the error distribution should be symmetric around line A–C, the 100 errors per position have additionally been mirrored around this symmetry line, so that a symmetrical pattern was obtained with 200 simulations per position. Fig. 5a and b shows the resulting spatial error map of the median (p_{50}) and maximal (p_{95}) error respectively. The axis coordinates adhere to the system used in Table 1, and the white dots indicate positions A–G. Position B at (1.25;1.25) is not indicated to better visualize the rapid variation of the error at that location. The median error over the entire area equals 4.21 cm, the maximal (p_{95}) error 10.75 cm.

Fig. 5a shows that the largest median (p_{50}) errors are found under the LED (7–9 cm), but at the exact location under the LED (position B), the error remains limited to 3.3 cm (see Table 2 and the bluish spot in the middle of the red area in Fig. 5a). Further, median errors appear to be larger along the sides of the square that is formed by the four LEDs and toward the corners. Unlike for the median errors, the largest maximal (p_{95}) errors in Fig. 5b do occur exactly below the LED (26.7 cm, see also Table 2). With respect to position F, Fig. 5a and b shows that although larger median errors are observed to the right of position F (for x around 1.5 m, see Fig. 5a), maximal errors are large exactly in F (x around 1.25 m, see Fig. 5b).

5.2. Alternative cost function

To better understand the spatial behavior of Fig. 5, a scatter plot of the estimated location for 100 locations in the same area as Fig. 5 (top right corner of the area) is shown in Fig. 6a. The white-edged dots in each point cloud indicate the real position, the larger orange dots indicate positions A–G. Fig. 6a again illustrates the symmetry along line A–B–C. As mentioned before, error clouds are more irregular around location B (middle of the figure), corresponding with the red cloud. Fig. 6a further shows that locations around B are drawn toward B. This can be explained when looking at the used cost metric (Eq. (5)). For locations near B, the absolute values of $P_{\mathrm{Ri}}^{\mathrm{obs}}$ and $P_{\mathrm{Ri}}^{L,\mathrm{model}}$ will be large for $i = i_B$, with i_B defined as the index number of the LED right above B. Since LED power tolerances are not absolute, but relative to the tabulated power, the factor $(P_{\mathrm{Ri}}^{\mathrm{obs}} - P_{\mathrm{Ri}}^{L,\mathrm{model}})^2$ in the cost metric will also be large for $i = i_B$. This makes that, near B, the power received from the LED above B has a larger influence on the global cost value than the power received

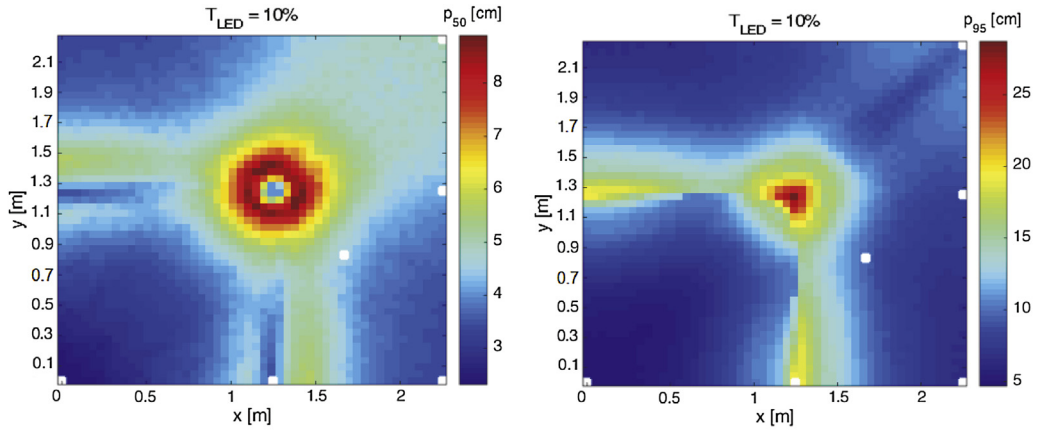

(a) Median error p_{50} (b) Maximal error p_{95}

Fig. 5. Spatial error distribution obtained from 200 simulations in the square A–C–E of Fig. 3a, for a LED tolerance value of 10% (white dots indicate locations A–G, except B).

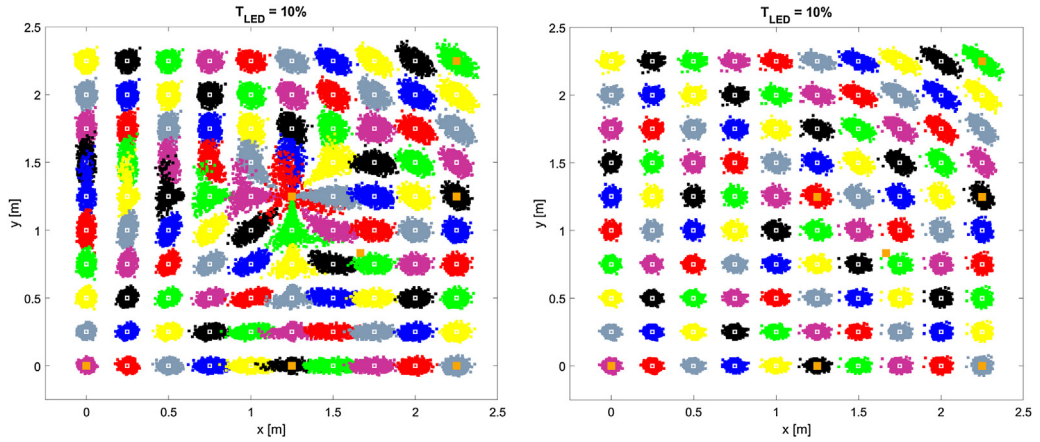

(a) Using traditional Least-Squares metric of eq. (5) (b) Using alternative normalized Least-Squares metric of eq. (8)

Fig. 6. Scatter plots of 1000 location estimations for each of 100 locations (indicated by white-edged dots) in the square A–C–E of Fig. 3a, for a LED tolerance value of 10% (orange dots indicate locations A–G). (For interpretation of the references to color in this figure legend, the reader is referred to the web version of this article.)

from the three other LEDs. Further, since we assume a Gaussian LED power distribution, the actual emitted power of the LED above B will be larger than the tabulated power in half of the cases. Since for $i = i_B$ (the LED above B), $P_{\text{Ri}}^{L,\text{model}}$ is maximal in B (for L = B), the cost function will draw the estimated location toward B for this half of the $P_{\text{Ri}}^{\text{obs}}$ values that are larger than those obtained from the tabulated transmit powers. This behavior is indeed observed in Fig. 6a and in Fig. 5a. In B itself, half of the times, location B is indeed favored, leading to the aforementioned low median errors. In case the actual transmit power for the LED above B is lower than the tabulated value (other half of the cases), the location is drawn away from B. Given the aforementioned large contribution of $(P_{\text{Ri}}^{\text{obs}} - P_{\text{Ri}}^{L,\text{model}})^2$ in the cost function for $i = i_B$, the location is drawn away relatively far, further supported by the lower gradient of the LED's radiation pattern around B in the (x, y)-plane.

To counter this effect, an alternative cost metric to Eq. (5) is proposed. To reduce the effect of the large influence of one LED in the area right below it, the received power values are normalized in the alternative cost metric:

$$C_{\text{square}}^{L} = \sum_{i}^{N} \left(\frac{P_{\text{Ri}}^{\text{obs}} - P_{\text{Ri}}^{L,\text{model}}}{P_{\text{Ri}}^{L,\text{model}}} \right)^2. \tag{8}$$

Fig. 6b shows the same scatter plot of the estimated locations, but using the alternative cost metric (Eq. (8)). It is shown that a much more homogeneous error distribution is obtained, without the high maximal errors that were previously found around B. Fig. 7 shows the spatial error maps of the median (p_{50}) and maximal (p_{95}) error for the alternative cost metric. Compared to the median

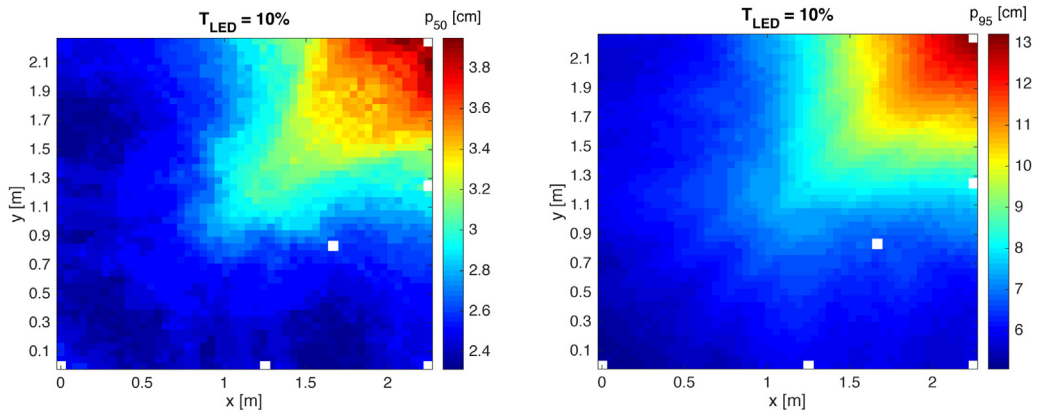

(a) Median error p_{50} (b) Maximal error p_{95}

Fig. 7. Spatial error distribution obtained from 200 simulations in the square A–C–E of Fig. 3a, for a LED tolerance value of 10% (white dots indicate locations A–G, except B), using the alternative cost function.

error over the entire area of 4.21 cm, and the maximal (p_{95}) error of 10.75 cm using the traditional cost metric (see Fig. 5), the alternative metric yields a median error of 2.61 cm and a maximal error of 6.99 cm over the same area, a reduction of 38% (median) and 35% (p_{95}). Fig. 7 shows that especially inside the LED square, errors remain limited.

5.3. Comparison with impact of noise and reflections

Fig. 8 shows the median positioning error for each of the seven considered locations, as a function of the standard deviation σ_N [W] of the observed noise power (without uncertainty on the LED power). It shows that from σ_N values of around 10^{-7} W and higher, the median error becomes larger than 1 cm. Location C (the furthest from the LEDs) is most prone to errors due to noise, while A (at the center of the 4 LEDs) is most resilient to noise. In our lab, a σ_N of around $1.4 \cdot 10^{-7}$ W was obtained. Table 3 shows the median (p_{50}) and maximal (p_{95}) values of the errors at the seven locations, considering LED power uncertainty and an assumed value of $\sigma_N = 1.4 \cdot 10^{-7}$ W. The table shows that at locations A, E, and G (the locations where noise has the lowest impact according to Fig. 8), the increase of the errors with respect to the errors listed in Table 2 (i.e., without considering noise) is indeed very limited: average errors increase at most 2%. At locations B, D, and F, an average error increase between 6 and 10% is noticed. At location C, Fig. 8 showed that noise had the largest impact on the positioning error. This is confirmed in Table 3: errors increase by 51%. On average, the relative impact of adding noise is obviously larger for lower T_{LED} values.

In realistic environments, the visible light channel will be altered due to walls, furniture, people, … [20]. In [18], the impact of reflections on the positioning accuracy was simulated for the same configuration, assuming diffuse reflections on the entire surface of all four side walls. One bounce was considered. The median and maximal errors obtained for this configuration due to a LED tolerance of 10% were equal to 4.21 and 10.75 cm, respectively. Using the same traditional Least-Squares cost metric 'square' [18], the median and maximal errors due to reflections amounted to 8.7 and 11.6 cm respectively, when a wall reflectance factor of 0.3 is assumed. It can be concluded that for the given configuration, the impact of noise is smaller than that of the LED power uncertainty, although the noise impact also becomes significant when moving further away from the LEDs. The impact of reflections is more or

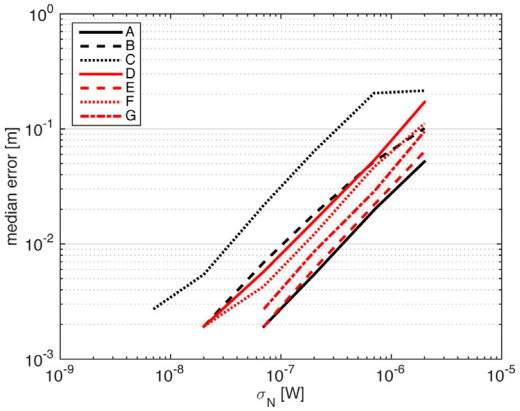

Fig. 8. Impact of noise on positioning accuracy for different positions.

Table 3
Median (p_{50}) and maximal (p_{95}) errors (cm) at each of the seven locations A–G (see Fig. 3a) for four tolerance values T_{LED} of the LEDs and a σ_N value of $1.4 \cdot 10^{-7}$ W.

T_{LED}		A	B	C	D	E	F	G
5%	p_{50}	1.2	2.2	5.0	2.3	1.7	1.7	2.3
	p_{95}	2.5	17.4	13.7	5.0	3.5	6.0	5.3
10%	p_{50}	2.3	3.7	6.5	4.0	3.3	3.2	4.6
	p_{95}	4.9	26.9	16.7	8.8	7.0	20.6	10.6
15%	p_{50}	3.5	4.9	8.4	5.9	4.9	4.9	6.8
	p_{95}	7.2	33.4	18.9	12.9	10.4	29.8	15.7
20%	p_{50}	4.6	5.8	10.5	7.7	6.5	6.7	9.0
	p_{95}	9.6	39.4	20.5	16.7	13.8	37.2	20.4

less comparable to that of a tolerance on the LED power of 10%.

5.4. 3D positioning

Fig. 9a, b, c, and d shows the cdfs that are obtained from 10^4 simulations at each of the locations A to F in Fig. 3b, for tolerances T_{LED} of 5, 10, 15, and 20%, respectively, for a PD receiver height of 0.85 m (which is unknown by the algorithm). Table 4 lists the median (p_{50}) and 95%-percentile (p_{95}) values of the errors for the six locations and four tolerance values, for two PD receiver heights ($h = 0.85$ m and $h = 3$ m). At $h = 0.85$ m, and for $T_{LED} = 5\%$, median errors are 5.6 cm at most (in B and C). Maximal errors are limited to 11.3 cm (B). At $h = 3$ m, and for $T_{LED} = 5\%$, median errors are 2.8 cm at most (in C and D). Maximal errors are limited to

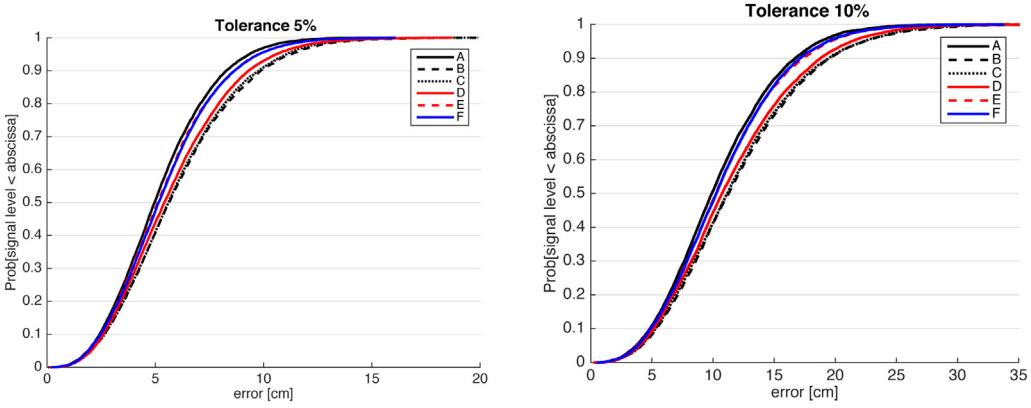

(a) LED tolerance value of 5%

(b) LED tolerance value of 10%

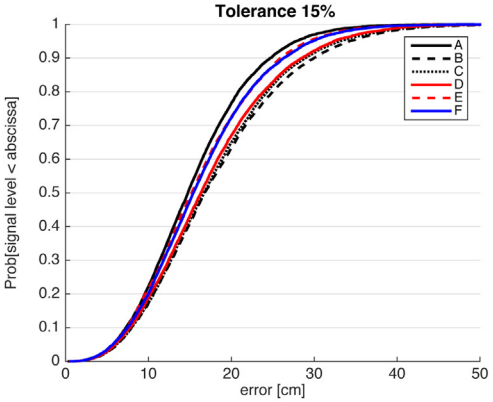

(c) LED tolerance value of 15%

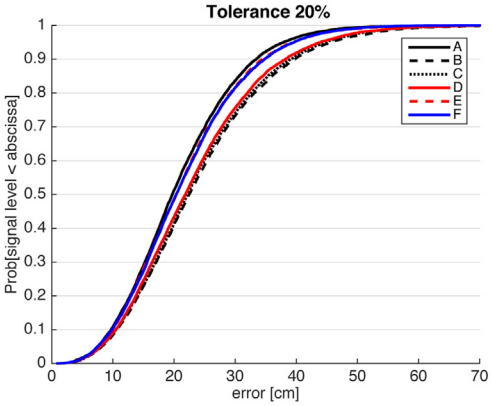

(d) LED tolerance value of 20%

Fig. 9. 3D cdfs of the errors obtained from 10 000 simulations at the locations A–F at $h = 0.85$ m.

Table 4
Median (p_{50}) and maximal (p_{95}) errors (cm) at each of the six locations A–F (see Fig. 3b) for four tolerance values T_{LED} of the LEDs and for two PD receiver heights (h = 0.85 m and h = 3 m).

h = 0.85 m							
T_{LED}		A	B	C	D	E	F
5%	p_{50}	5.0	5.6	5.6	5.4	5.1	5.2
	p_{95}	9.3	11.3	11.1	10.6	9.8	9.8
10%	p_{50}	9.9	11.3	11.2	10.7	10.2	10.3
	p_{95}	18.8	22.4	22.3	21.3	19.6	19.4
15%	p_{50}	14.8	16.8	16.7	16.3	15.2	15.4
	p_{95}	27.8	34.2	33.1	32.4	29.3	29.8
20%	p_{50}	19.7	22.5	22.2	21.8	20.4	20.3
	p_{95}	37.9	45.6	44.8	43.9	39.4	39.6
h = 3 m							
T_{LED}		A	B	C	D	E	F
5%	p_{50}	2.2	3.0	2.8	2.8	2.5	2.5
	p_{95}	4.1	7.1	5.8	6.1	4.8	5.0
10%	p_{50}	4.5	6.2	5.6	5.6	5.0	5.0
	p_{95}	8.3	14.7	11.4	12.2	9.6	10.2
15%	p_{50}	6.8	9.3	8.5	8.3	7.5	7.5
	p_{95}	12.6	21.6	18	18.1	14.3	15.2
20%	p_{50}	9.1	12.3	11.3	11.2	9.9	10.0
	p_{95}	17.1	28.5	23.4	24.7	19.6	20.5

7.1 cm (B).

All median errors scale very much linearly with the tolerance values: the errors increase between 97 to 107%, 196 to 210%, and 290 to 317%, when T_{LED} increases from 5% to 10, 15, and 20%, respectively (for h = 0.85 and 3 m). Errors at h = 3 m are consistently lower than at h = 0.85 m: over all T_{LED} values and positions, median errors at h = 3 m are 45 (in B) to 56% (in A) lower, and maximal errors 37 (in B) to 56% (in A). The reason is that the gradient of the received powers in the (x, y)-plane is higher closer to the LEDs (i.e., for larger h values), so that a larger area of the N-dimensional space of P_{Ri} values (i = 1, …, N, N = 4 here) is used, and deviations on the LED powers have a smaller impact on the positioning error. Fig. 9a, b, c, and d indeed shows the linear increase of the positioning errors at positions A to F, as a function of T_{LED}. The set of cdfs look very similar in the different figures, but are stretched horizontally, i.e., they correspond to increasing errors.

The presented values in Table 4 suggest that smaller errors are obtained for positions closer to the central LED (position A): errors in E and F are larger than in A, but smaller than in B, C, and D (see also Fig. 3b). To verify this assumption, median and maximal errors for T_{LED} = 10% within the top half of Fig. 3b (above line A–C) have been simulated on a grid of 100 by 50 positions, at a PD receiver height of 0.85 m. Due to calculation time, the number of simulations per location is limited to 1000 instead of 10 000. The resulting error distribution is symmetric around line A–C, due to the layout of the LED configuration (see Fig. 3b). Figs. 10 and 11 show the spatial error map of the median (p_{50}) and maximal (p_{95}) error in the considered area, respectively. The axis coordinates adhere to the system used in Table 1, and the white dots indicate positions A–F. The median error over the entire area equals 11.00 cm, the maximal error 22.23 cm.

Figs. 10 and 11 indeed show that the smallest median and maximal errors are found near position A (9.91 and 18.32 cm in A), and increase gradually toward the edges of the room. When comparing median and maximal errors, the same spatial pattern is observed, leading to seemingly almost identical figures. When comparing Figs. 10 and 11 with the corresponding 2D figures (Fig. 5a and b), it is seen that the 3D configuration/algorithm shows a smoother global error trend than the 2D setup/algorithm (see the very local maxima in B in Fig. 5a and b). At a smaller scale however, the 3D case shows larger variations between adjacent evaluation points (which are 5 cm apart) than the 2D case (see the speckled pattern in Figs. 10 and 11). Compared to the 2D case, the 3D configuration leads to median and maximal errors within a relatively limited range: median errors are between 9.5 cm and 13.5 cm, and maximal errors between 18 and 30 cm.

6. Conclusions

In this paper, it is investigated to what extent the uncertainty or tolerance on the actual emitted LED power impacts the RSS-based VLP accuracies, both for a 2D and 3D configuration. For a 5 m × 5 m room with four LEDs, the distributions of the resulting positioning errors are evaluated, based on a Monte Carlo simulation consisting of 10^4 simulations. For the 2D case, median errors are below 2.5 cm at most locations for a tolerance of 5%, and these errors increase approximately linearly as the tolerance values on the LED powers increase, with most median errors below 10 cm for a tolerance of 20%. However, it is shown that median and maximal

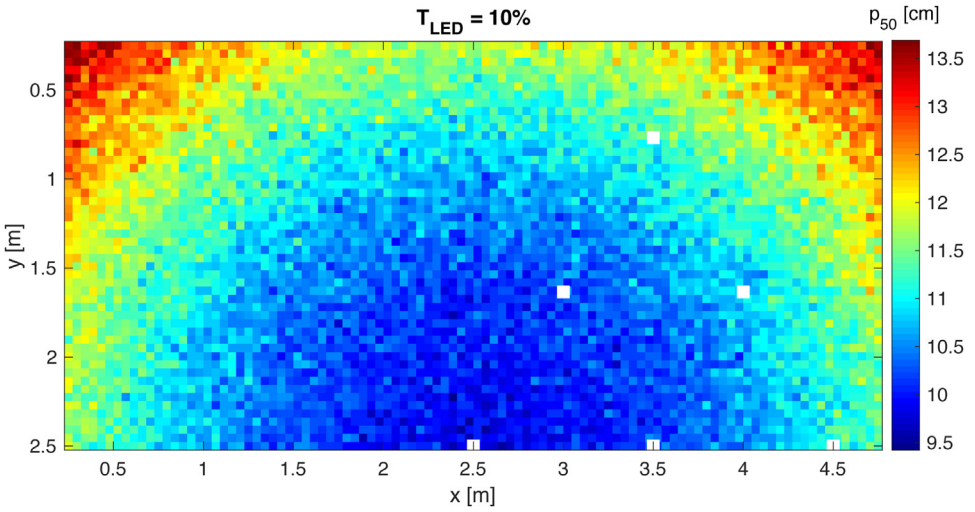

Fig. 10. Spatial distribution of median (p_{50}) error, obtained from 100 simulations in the upper half of the configuration of Fig. 3b, for a LED tolerance value of 10% (white dots indicate locations A–F).

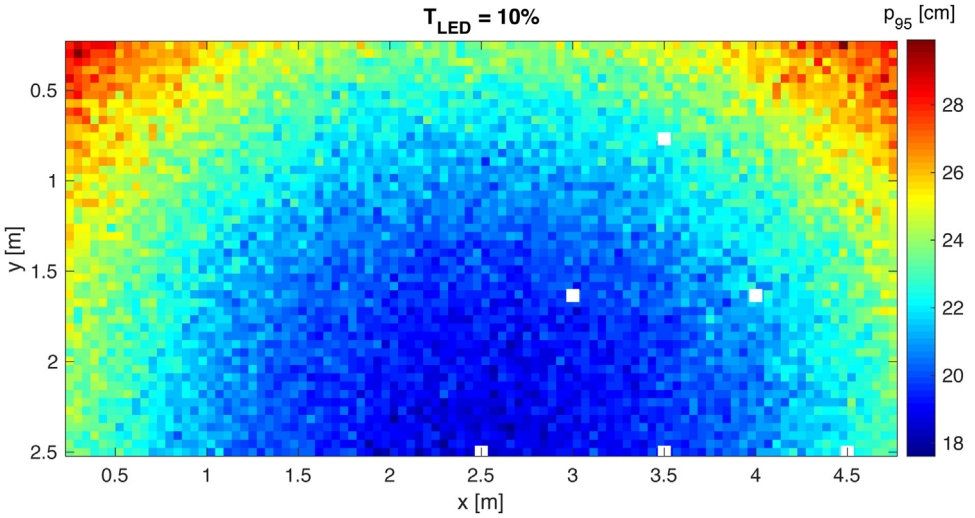

Fig. 11. Spatial distribution of 95%-percentile (p_{95}) error, obtained from 100 simulations in the upper half of the configuration of Fig. 3b, for a LED tolerance value of 10% (white dots indicate locations A–F).

errors show significant local variations, where the highest positioning errors are observed at locations just below the LEDs. For tolerance values of only 5%, maximal errors can already be as high as 17 cm just below the LED, and increase up to 40 cm for tolerance values of 20%. An alternative cost metric using normalized received power is proposed, which reduces aforementioned impact. For the considered configuration, a tolerance value of 10% has an impact on positioning accuracy that is comparable to that of wall reflections, and has a larger impact than noise. For the investigated 3D case, median errors increase from around 5 cm for a tolerance value of 5% to as much as 22 cm for a tolerance value of 20%. As the receiver height increases from 85 cm to 3 m, positioning errors decrease significantly, with median errors around 2.5 cm for a tolerance value of 5%, up to 12 cm for a tolerance value of 20%.

Future work includes an experimental analysis of actual LED power tolerances and LED positions. Further, the impact on the error will be investigated when the powers of the different LEDs are correlated, since LEDs from a same batch might be likely to have similar deviations from the tabulated power. Also, the 2D study can be repeated for commercial LED sources instead of Lambertian radiators.

Acknowledgments

This work was executed within LEDsTrack, a research project bringing together academic researchers and industry partners. The LEDsTrack project was co-financed by imec (iMinds) and received project support from Flanders Innovation & Entrepreneurship.

References

[1] A. Jovicic, J. Li, T. Richardson, Visible light communication: opportunities, challenges and the path to market, IEEE Commun. Mag. 51 (12) (2013) 26–32, https://doi.org/10.1109/MCOM.2013.6685754.

[2] J. Armstrong, Y.A. Sekercioglu, A. Neild, Visible light positioning: a roadmap for international standardization, IEEE Commun. Mag. 51 (12) (2013) 68–73.

[3] D. Dardari, A. Conti, U. Ferner, A. Giorgetti, M.Z. Win, Ranging with ultrawide bandwidth signals in multipath environments, Proc. IEEE 97 (2) (2009) 404–426.

[4] J. Trogh, D. Plets, L. Martens, W. Joseph, Advanced real-time indoor tracking based on the Viterbi algorithm and semantic data, Int. J. Distrib. Sens. Netw. 11 (10) (2015), https://doi.org/10.1155/2015/271818.

[5] D. Wu, Z. Ghassemlooy, W.-D. Zhong, M.-A. Khalighi, H.L. Minh, C. Chen, S. Zvanovec, A.C. Boucouvalas, Effect of optimal Lambertian order for cellular indoor optical wireless communication and positioning systems, Opt. Eng. 55 (6) (2016) 1–8, https://doi.org/10.1117/1.OE.55.6.066114.

[6] K. Saxena, R. Raj, A. Dixit, 2018 9th International Conference on Computing, Communication and Networking Technologies (ICCCNT), (2018), pp. 1–7, https://doi.org/10.1109/ICCCNT.2018.8493666.

[7] D. Li, C. Gong, Z. Xu, A RSSI-based indoor visible light positioning approach, 2016 10th International Symposium on Communication Systems, Networks and Digital Signal Processing (CSNDSP) (2016) 1–6, https://doi.org/10.1109/CSNDSP.2016.7574003.

[8] T. Yuan, Y. Xu, Y. Wang, P. Han, J. Chen, A tilt receiver correction method for visible light positioning using machine learning method, IEEE Photonics J. 10 (6) (2018) 1–12, https://doi.org/10.1109/JPHOT.2018.2880872.

[9] D. Plets, S. Bastiaens, L. Martens, W. Joseph, An analysis of the impact of LED tilt on visible light positioning accuracy, Electronics 8 (4) (2019), https://doi.org/10.3390/electronics8040389.

[10] M.F. Keskin, A.D. Sezer, S. Gezici, Optimal and robust power allocation for visible light positioning systems under illumination constraints, IEEE Trans. Commun. 67 (1) (2019) 527–542, https://doi.org/10.1109/TCOMM.2018.2866849.

[11] TCI Telecomunicazioni, CD MAXI JOLLY DALI, Tech. rep. http://www.tcisaronno.com/PDF/istruzioni/DC_MAXI_JOLLY_DALI.pdf.

[12] Citiled, Citiled COB CLU038-1205C4 Datasheet, Tech. rep. http://ce.citizen.co.jp/lighting_led/dl_data/datasheet/en/COB_5/CLU038-1205C4_P3537_0216.pdf.

[13] D. Plets, S. Bastiaens, N. Stevens, L. Martens, W. Joseph, Monte-Carlo simulation of the impact of LED power uncertainty on visible light positioning accuracy, 11th International Symposium on Communication Systems, Networks & Digital Signal Processing, CSNDSP 2018, Budapest, Hungary, July 18–20, 2018, pp. 1–6, , https://doi.org/10.1109/CSNDSP.2018.8471838.

[14] S.-H. Yang, E.-M. Jeong, D.-R. Kim, H.-S. Kim, Y.-H. Son, S.-K. Han, Indoor three-dimensional location estimation based on LED visible light communication, Electron. Lett. 49 (1) (2013) 54–56, https://doi.org/10.1049/el.2012.3167.

[15] T. Komine, M. Nakagawa, Fundamental analysis for visible-light communication system using LED lights, IEEE Trans. Consum. Electron. 50 (2004) 100–107.

[16] S.D. Lausnay, L.D. Strycker, J.-P. Goemaere, N. Stevens, B. Nauwelaers, A Visible Light Positioning system using Frequency Division Multiple Access with square waves, 2015 9th International Conference on Signal Processing and Communication Systems (ICSPCS), Cairns, QLD, Australia, 2015, pp. 1–7.

[17] D. Plets, Y. Almadani, S. Bastiaens, M. Ijaz, L. Martens, W. Joseph, Efficient 3D trilateration algorithm for visible light positioning, J. Opt. (2019), https://doi.org/10.1088/2040-8986/ab1389.

[18] D. Plets, A. Eryildirim, S. Bastiaens, N. Stevens, L. Martens, W. Joseph, A performance comparison of different cost functions for RSS-based visible light positioning under the presence of reflections, Proceedings of the 4th ACM Workshop on Visible Light Communication Systems at the 23rd Annual International Conference on Mobile Computing and Networking, ACM Press, 2017, pp. 37–41, , https://doi.org/10.1145/3129881.3129888.

[19] S. Bastiaens, D. Plets, L. Martens, W. Joseph, Response adaptive modelling for reducing the storage and computation of RSS-based VLP, 2018 International Conference on Indoor Positioning and Indoor Navigation (IPIN) (2018) 1–8, https://doi.org/10.1109/IPIN.2018.8533750.

[20] P. Chvojka, S. Zvanovec, P.A. Haigh, Z. Ghassemlooy, Channel characteristics of visible light communications within dynamic indoor environment, J. Lightwave Technol. 33 (9) (2015) 1719–1725, https://doi.org/10.1109/JLT.2015.2398894.